Eur. Phys. J. AP **18**, 221–227 (2002)
DOI: 10.1051/epjap:2002042

THE EUROPEAN PHYSICAL JOURNAL
APPLIED PHYSICS

Supersonic Fe beam source for chromatic aberration-free laser focusing of atoms

R.C.M. Bosch, H.C.W. Beijerinck, P. van der Straten, and K.A.H. van Leeuwen[a]

Department of Applied Physics, Eindhoven University of Technology, PO Box 513, 5600 MB Eindhoven, The Netherlands

Received: 20 November 2001 / Received in final form: 6 March 2002 / Accepted: 26 March 2002
Published online: 6 June 2002 –

Abstract. A monochromatic Fe beam is generated by heated supersonic expansion of argon seeded with Fe vapor. At a nozzle temperature of 1930 K and 800 torr argon inlet pressure the Fe beam has an axial velocity spread of 8% and intensity of 3×10^{15} $s^{-1}\,sr^{-1}$, corresponding to a deposition rate of 10 nm/h at 150 mm from the nozzle. The two-chamber alumina crucibles are chemically stable for liquid Fe. With 400 mm^3 Fe we have operated for more than 200 hours without reloading. The power consumption at 1930 K is 750 W. Temperature stability at constant power (without feedback) is better than 30 K. The source is intended for deposition of nanostructures by laser focusing of the Fe beam. The small axial velocity spread virtually eliminates the increase in focal spot size due to chromatic aberration.

PACS. 39.10.+j Atomic and molecular beam sources and techniques – 32.80.Lg Mechanical effects of light on atoms, molecules, and ions – 39.25.+k Atom manipulation (scanning probe microscopy, laser cooling, etc.)

1 Introduction

Laser focusing of atoms for the production of periodic nanostructures is increasingly gaining interest. Arrays of lines and dots have been produced by etching with metastable atoms, He* [1,2], Ne* [3], and Ar* [4], etching with alkali atoms, Na [5] and Cs [6], and by deposition of metal atoms, Cr [2,7] and Al [8]. The supersonic Fe source which is presented in this paper has been developed for the fabrication of periodic structures of Fe by laser focusing. This particular atom has been chosen for its ferromagnetic properties. The fabrication of arrays of nanometer-sized Fe lines and dots would provide an experimental entry into a new fascinating field of 1D and 0D nanomagnetics [9].

The technique of laser focusing for the production of these nanostructures requires a well defined atomic beam. Just as in conventional optics the quality of the focused image is limited by initial beam collimation and chromatic aberration. These two aspects are determined by the initial spread in transverse velocity of the atomic beam and the spread in axial velocity of the atoms, respectively. Thus, for a controlled deposition of arrays the Fe beam needs to be collimated and "monochromatic" (single-axial-velocity). The first property can be established by aperturing the beam or by transverse Doppler cooling [10], resulting in beams collimated below 0.1 mrad. Monochromatic beams can be generated by Zeeman slowing of a thermal beam [5], or by using a supersonic beam [11]. The relatively low axial velocity spread in a supersonic beam is characterized by a high speed ratio S, defined by the ratio of the average axial velocity to the axial velocity spread. In experiments on laser focusing of metal atoms as Cr and Al, the atomic beam is generated by an effusive source, resulting in a thermal beam with an axial velocity spread comparable to the average velocity. In this case, the effect of chromatic aberration is rather drastic, as the focal length scales quadratically with the axial velocity of the atoms. The lack of monochromatic beams of metal atoms is therefore one of the reasons that structures below 10 nm have not yet been produced. Calculations on laser focusing of a collimated Fe beam of 0.1 mrad show that the focal spot size decreases from 15 nm to 8 nm if a supersonic rather than a thermal beam is used [12].

This paper will describe the development of a supersonic Fe evaporation source. Supersonic beam sources for high-melting-point metals such as Fe are uncommon, because they pose special construction problems due to the required high temperature, large pressure and small exit nozzle. Expertise in this field was developed by the group of Hagena [13]. We have used the basic concept of their high temperature evaporation source for the generation of metal cluster beams. The result is the construction of a supersonic Fe evaporation source, containing a crucible which is chemically stable with molten Fe at temperatures well above 2000 K, and an oven with small temperature gradients to prevent diffusion of Fe and nozzle clogging. A supersonic Fe beam with center line intensities of up to 10^{16} atoms $s^{-1}\,sr^{-1}$ can be generated. With these intensities, the deposition rate of structures is at least 20 nm/h

[a] e-mail: K.A.H.v.Leeuwen@tue.nl

at 150 mm from the nozzle, requiring a background pressure of 10^{-9} torr or lower to minimize contamination.

2 Seeded supersonic expansions

Supersonic beams are obtained by expanding a relatively high pressure ($p_0 \sim 10$–10^4 torr) gas through a small nozzle into vacuum [14]. Producing such an expansion from pure Fe vapor is not practical, requiring an unrealistically high temperature. Thus, we use Ar as a high pressure carrier gas into which Fe is seeded at a moderate pressure. Other noble gases such as He or Ne could also be used. However, the resulting beam velocity (which is determined by the thermal velocity of the carrier gas) would be too high for adequate laser cooling and laser focusing. The Ar flux $\dot{N}$ (atoms/s) and undisturbed Ar center line intensity I_0^{id} (atoms/s/sr) are given by [11]

$$\dot{N} = 0.513\, n_0 \alpha_0 (\pi d^2/4) \tag{1}$$

$$I_0^{id} = \kappa \dot{N}/\pi, \tag{2}$$

where $n_0 = p_0/kT_0$ is the reservoir density, $\alpha_0 = (2kT_0/m)^{1/2}$ the thermal velocity and d the nozzle diameter. For sonic nozzles the value of the peaking factor κ is equal to 2.08 [11]. Due to the high reservoir pressure the flow of the expansion is continuous during the first few nozzle diameters. In the expansion both the local temperature $T(z)$ and local density $n(z)$ decrease with the distance z from the nozzle. Most of the thermal energy of the atoms in the reservoir will be transferred to kinetic energy in the direction of propagation, leading to the lowering of the local temperature and to an increase in the flow velocity. At some point, a few nozzle diameters from the nozzle, the stream lines become straight lines resulting in a radial expansion with an angular intensity distribution $I_\theta \propto \cos\theta^3$, with θ the angle with respect to the center-line of the expansion. A back projection of these stream lines onto the nozzle plane results in a Gaussian distribution with a rms width defined as the virtual source radius R_v [11]. When the beam is collimated by a pinhole some distance downstream, the virtual source radius (almost identical for Fe and Ar) determines the divergence of the transmitted beam.

When the local density becomes so low that collisions are no longer significant, the atoms move freely in straight line trajectories. The parallel temperature freezes [11] and is given by $kT_\parallel = \frac{1}{2} m \alpha_\parallel^2$. The axial velocity distribution of the supersonic beam is then given by

$$P(v) \propto \left(\frac{v}{u}\right)^3 \exp\left[-\left(\frac{v-u}{u}\right)^2 S^2\right], \tag{3}$$

with the speed ratio S is defined as the ratio of the final flow velocity u to the final parallel velocity spread $\alpha_\parallel$. The final flow velocity can be calculated from the enthalpy balance given by $\frac{5}{2}kT_0 = \frac{1}{2}mu^2 + \frac{3}{2}kT_\parallel$, resulting in

$$u = u_\infty \left(1 + \frac{3}{2}S^{-2}\right)^{-1/2}, \tag{4}$$

with $u_\infty = (5kT_0/m)^{1/2}$ the final flow velocity for $S \to \infty$. Speed ratios of supersonic beams have been measured and calculated extensively [16]. The most widely used theoretical predictions are based on the sudden freeze model [11], resulting in

$$S = 19.1 \left(\frac{\Xi}{100}\right)^{0.495}, \tag{5}$$

where Ξ is the reservoir parameter which depends on the nozzle diameter d, the inlet pressure p_0 and oven temperature T_0. For Ar the reservoir parameter Ξ can be expressed as [11]

$$\Xi = 100 \left(\frac{d}{0.2\text{ mm}}\right)\left(\frac{p_0}{170\text{ torr}}\right)\left(\frac{T_0}{300\text{ K}}\right)^{-4/3}. \tag{6}$$

Background pressures in the expansion chamber are on the order of 10^{-1} torr, due to the large gas load into the vacuum system ($\dot{N} > 10^{20}$ atoms/s). As a result strong shock waves appear at the boundaries of the Campargue-type expansion [15] and a conical skimmer has to be used to extract an atomic beam on the center line carefully without excessive loss of beam intensity. Inside the skimmer tip the beam is attenuated according to Beer's law, i.e., an exponential decrease with an exponent scaling with the local inverse Knudsen number Kn^{-1}. Since this number is proportional to the inlet pressure p_0, scattering with background Ar atoms inside the skimmer tip leads to an exponential decrease of beam intensity with p_0 [16]:

$$I_0 = I_0^{id} \exp\left[-q p_0\right]. \tag{7}$$

A supersonic Fe beam is obtained by heating Fe inside the reservoir to temperatures up to 2000 K, corresponding to Fe vapor pressures in the range of 10^{-2} to 10^{-1} torr. The Ar gas carries the Fe vapor and the mixture expands supersonically. If thermodynamic equilibrium between Ar and Fe is established in the continuum flow regime of the expansion, the beam velocities and beam temperature of both species will be equal and their values will be almost the same as for a pure Ar expansion. The speed ratio of Fe is then given by

$$\frac{S_{Fe}}{S_{Ar}} = \left(\frac{m_{Fe}}{m_{Ar}}\right)^{1/2} \tag{8}$$

and is 18% higher than the speed ratio of Ar (mass ratio of 56 over 40). However, equation (8) is an upper limit. Experimental values can differ significantly especially for heavier species, whose cooling process due to collisions with the much lighter carrier gas atoms is not that efficient. A closer look at the cooling of dilute binary mixtures in a supersonic expansion is given in [17], resulting in a modification of equation (8):

$$\frac{S_M}{S_m} = \left(\frac{M}{m}\right)^{1/2} \left[0.33\left(\frac{m}{M} - 1\right) + 1\right]^{1/2} \left(\frac{C_{6m}}{C_{6M}}\right)^{1/12}, \tag{9}$$

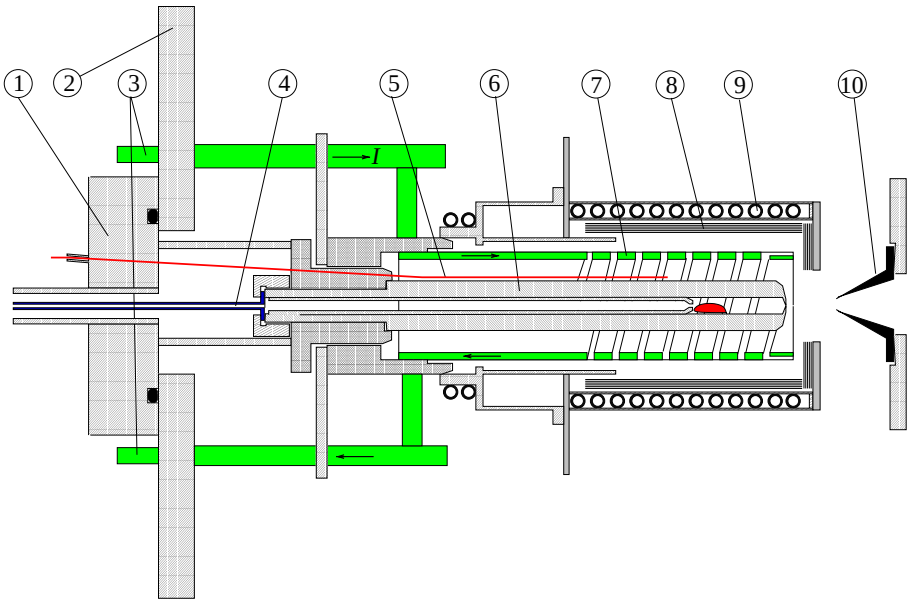

Fig. 1. Schematic view of the supersonic metal evaporation source: (1) flange with crucible unit, (2) flange with heating unit, (3) copper electrodes for DC heating, (4) tantalum tube for argon gas inlet, (5) WRe(3%/26%) thermocouple, (6) crucible, (7) heating coil, (8) radiation shields, (9) water cooled stainless steel mount, (10) graphite skimmer.

where M is the mass of the dilute heavy atoms, and m the mass of the light atoms driving the expansion. The second and third term of equation (9) represent the efficiency of the cooling of species with different masses and cross sections. For noble gases collision processes at low temperature are dominated by the long-range attractive branch of $V(r) \propto -C_6/r^6$ with C_6 the Van der Waals constant, resulting in cross sections that can be written as $(C_6/kT)^{1/3}$. For metal atoms such as Fe, the collision cross section has been estimated by experiments on metal cluster beams [18], leading to an artificial C_6 coefficient which is a factor of 6.3 larger than the C_6 coefficient of argon. Equation (9) then predicts an Fe speed ratio which is 3% lower than the Ar speed ratio.

The Fe beam intensity between nozzle and skimmer is just the undisturbed Ar beam intensity times the ratio of the Fe vapor pressure p_v to the Ar inlet pressure p_0:

$$I^{id}_{0,Fe} = \frac{p_v}{p_0} I^{id}_0, \tag{10}$$

which is independent of the argon inlet pressure p_0, since I^{id}_0 is proportional to p_0 according to equations (1, 2). Due to collisions between Fe atoms with Ar atoms at the skimmer tip, the Fe beam is attenuated by

$$I_{0,Fe} = I^{id}_{0,Fe} \exp\left[-q(C_{6M}/C_{6m})^{1/6} p_0\right], \tag{11}$$

with a different exponential decay factor than the argon beam attenuation according to equation (7), due to different cross sections of Fe and Ar represented by the coefficients C_{6M} and C_{6m}. Since the speed ratio of Fe increases with increasing p_0 according to equation (5) and the skimmer transmission decreases exponentially with p_0, a compromise has to be chosen between speed ratio and beam intensity.

3 Supersonic Fe beam source

Figure 1 shows a drawing of the supersonic Fe source. Different crucible materials have been tested for their thermal shock resistance and chemical stability with liquid Fe at $T > 1800$ K. The most important materials and the corresponding crucible constructions that have been tested are shown in Figure 2. Eventually, alumina crucibles with a nozzle diameter of 230 μm have been used.

The crucible is heated by a high density graphite heating coil. The coil is doubly wound with a large cross section of 3×5 mm^2, necessary because of the high electrical resistance of graphite. The last winding which is located at the nozzle has been made thin (1.5×5 mm^2) to increase the resistance power output, to keep the nozzle hotter than the rest of the crucible. The total resistance is 0.5 Ω, convenient for DC heating.

To minimize the input power and to reduce temperature gradients, 20 layers of wrapped tantalum foil heating shield are used in the radial direction and 5 layers at the nozzle side. An opening of 20 mm diameter allows an undisturbed supersonic expansion of the Ar gas. The outside stainless steel cylindrical mount is water cooled. With this construction, the main contribution to heat losses of the oven are radiative heat loss out of the front side opening and conduction heat loss through the heating coil.

The crucible assembly is a separate unit that can be removed from the heating unit very easily for maintenance or the reloading of metal. The heating coil has proven to be very stable and durable and has been run on and off for several years up to now without any signs of deterioration. The concept of a separate crucible assembly combined with a graphite heating coil, has been used by Hagena for the generation of metal cluster beams [13]. His design formed the basis of our Fe source design.

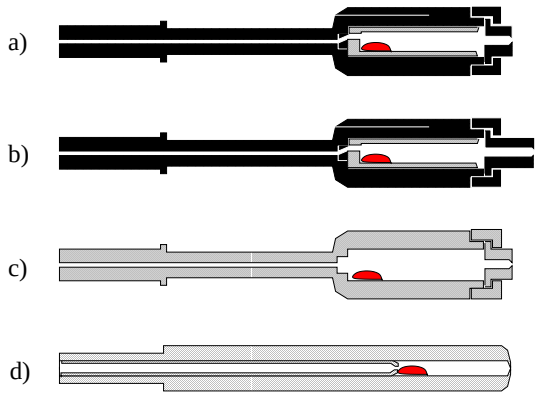

Fig. 2. Crucibles tested for the evaporation of different metallic elements. (a) High density graphite crucible with BN insert and threaded nozzle assembly with short nozzle, (b) high density graphite crucible with BN insert and longer nozzle, (c) BN crucible and nozzle assembly, (d) Al_2O_3 crucible with fixed nozzle on outside tube. The inside tube prohibits back diffusion of metal atoms.

High density graphite crucibles (as shown in Figs. 2a and 2b) were tested first, as graphite is easily machinable into a variety of different shapes, with a threaded nozzle assembly which makes reloading of metal very easy. The temperature was monitored using a WRe(3%/26%) thermocouple inserted in a small hole in the crucible wall at the position of the melt. However, problems arose at temperatures above the Fe melting point (1800 K), where molten Fe reacts with the graphite crucible wall at a rate of typically 0.1 mm/h. An insert in the graphite reservoir made of boron nitride (BN) increased the lifetime. However, the nozzle was attacked by Fe vapor, causing the nozzle size to increase by approximately 10% after ten hours of operation.

Crucibles made entirely of BN (Fig. 2c) were also tested. These crucibles can operate at slightly higher temperatures. However, above 2000 K deterioration by the molten Fe was also observed.

Highly purified alumina (>99.7%) (Fig. 2d) was found to have high tolerance to molten Fe. The maximum operating temperature was 2200 K, above which this material starts to sublimate. Alumina is difficult to machine, and in particular, the fabrication of the nozzle of 230 μm diameter could only be realized by laser ablation. The assembly consists of two alumina tubes, the smaller one with a 1 mm orifice inserted into the larger nozzle tube. This way diffusion of the molten metal into the gas feed is prohibited by a constant flow of Ar out of the 1 mm orifice into the reservoir. Because of the loose fit between the two tubes, Ar also flows in between the two tube walls into the reservoir and prevents the metal vapor from diffusing in between the tube walls. The smaller tube can also be removed easily, making a reload of metal possible. Table 1 gives an overview of the most relevant properties of the Fe source.

Table 1. Properties of the experimental setup and typical Fe/Ar beam properties.

Supersonic source		
operating temperature	T_0	300–2300 K
Ar inlet pressure	p_0	100–1200 torr
flow rate	$\dot{N}$	10^{19}–10^{20} s^{-1}
nozzle diameter	d	0.2–0.25 mm
skimmer diameter		0.5–0.8 mm
nozzle - skimmer distance		10–15 mm
beam attenuation parameter	q	8.6×10^{-4} torr^{-1}
Typical beam properties		
source temperature	T_0	1930 K
Ar inlet pressure	p_0	800 torr
Fe vapor pressure	p_v	0.1 torr
Ar beam intensity	$I_{0,Ar}$	2×10^{19} s^{-1} sr^{-1}
Fe beam intensity	$I_{0,Fe}$	3×10^{15} s^{-1} sr^{-1}
Ar speed ratio	S_{Ar}	11
Fe speed ratio	S_{Fe}	11
virtual source radius	R_v	0.25 mm
beam divergence	R_v/z ($z = 1$ m)	0.25 mrad
Time-of-flight setup		
flight path	L	1265 mm
beam chopper diameter		90 mm
slit #1 width		1.0 mm
slit #2 width		39 mm
chopping frequency		200 Hz

4 Experimental setup

The beam properties of Fe and seed gas Ar have been determined using a time-of-flight setup with a mass spectrometer as detector to measure the relative beam intensities of Fe and Ar. A calibration procedure was used in order to obtain absolute values. Undisturbed Ar beam intensities, *i.e.*, an ideal Ar beam that is not attenuated at the skimmer, can be calculated using equations (1, 2). However, experimental Ar beam intensities will be lower by a factor of $\exp(-qp_0)$ as given in equation (7). The parameter q of this factor can be determined by fitting the data shown in Figure 3. In this graph the Ar detector signal (left vertical axis) is shown for various Ar inlet pressures in the range of 100 to 1000 torr. The ideal beam intensity indicated by the dashed line is a straight line with a slope equal to the slope of the fit of the measured data serie at $p_0 = 0$. Absolute values for experimental beam intensities are obtained by multiplying the ideal beam intensity calculated with equation (2) with the decay factor $\exp(-qp_0)$. The result of the fit is given in Table 1.

The Fe beam intensity can be determined in two ways: first by multiplying the calibrated Ar beam intensity with the ratio of the detector signal of Fe to Ar, secondly with the ratio of the Fe vapor pressure to the Ar inlet pressure according to equations (10, 11).

Speed ratios of all species can be determined by time-of-flight measurements using a rotating slotted disk type mechanical beam chopper and a mass spectrometer. The beam chopper has two narrow slits of 1 mm for the time-of-flight measurements and two wide slits of 39 mm which transmit the full beam. The chopper gate time of the small slit is much shorter than the average time the atoms need to reach the detector. This way the measured

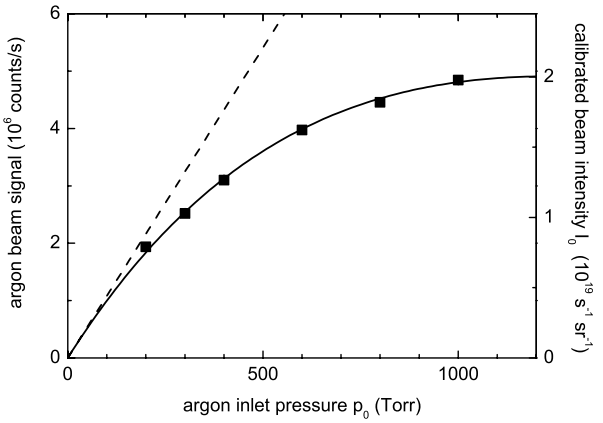

Fig. 3. Calibration of the argon beam intensity I_0. The ideal beam intensity (dashed line) is linear with the inlet pressure and can be calculated using equation (2), whereas the disturbed beam intensity as measured is lower by a factor $\exp(-qp_0)$. Absolute values for the Ar beam intensity can be obtained by fitting the measured data with equation (7). Nozzle temperature is 1930 K.

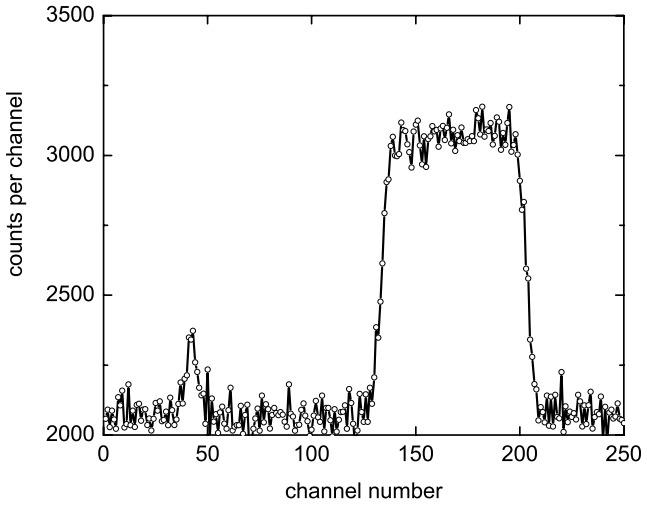

Fig. 4. Measured time-of-flight distribution of Fe atoms at $T_0 = 1930$ K and $p_0 = 800$ torr. The small peak gives the flow velocity and speed ratio of the Fe beam when fitting with equation (12). The large peak gives the Fe beam intensity. The distribution is obtained by a summation of 60 000 TOF-sweeps collected in a multiscaler with a channel time of 20 μs.

time-of-flight signal directly reflects the velocity distribution of the beam. For a density sensitive detector such as the ionization detector of the mass spectrometer, this signal is

$$N(t) \propto t^{-4} \exp\left[-S^2\left(\frac{L}{ut}-1\right)^2\right]. \qquad (12)$$

The flow velocity u and speed ratio S can be determined by fitting the measured time-of-flight distribution with equation (12). The nozzle temperature follows from the flow velocity u by equation (4). Figure 4 shows an example of a time-of-flight distribution of Fe. The distribution is obtained by a summation of 60 000 TOF-sweeps collected in 250 channels of a multiscaler with a channel time of 20 μs. The small peak in the distribution can be fitted to equation (12) to obtain the flow velocity and speed ratio. The large peak, transmitted by the wide slits of the chopper, provides a measure of the full beam intensity if the detection efficiency is known. In this measurement the full Fe beam signal is 830 counts/s. Properties of the time-of-flight setup are listed in Table 1.

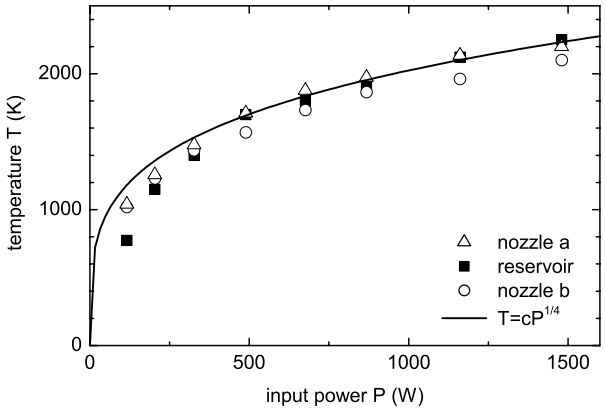

Fig. 5. Reservoir and nozzle temperature T at increasing input power P. Reservoir temperatures have been measured with a thermocouple. Nozzle temperatures have been measured by time-of-flight analysis. The shorter, recessed nozzle (a) is significantly hotter than the longer nozzle (b), with temperatures exceeding the reservoir temperature, thus preventing nozzle clogging. The solid line gives the radiative heating loss dependence $T \propto P^{1/4}$ and shows that at high temperatures radiative heating loss is dominant. Losses due to thermal conductivity, which scale as $T \propto P$, are more important at low temperatures.

5 Results

Figure 5 shows the results of DC heating of the source. Due to the careful radiation shielding, temperatures up to 2200 K can be reached at relatively low input powers of less than 1500 W. Figure 5 shows three temperature curves. One curve has been measured by a thermocouple inserted in the graphite crucible wall. This is a measure of the reservoir temperature and therefore the temperature of the metal vapor. Temperature stability is within 25 K. The reproducibility is within 25 K over the last two years.

The other two curves in Figure 5 represent the nozzle temperature as measured with time-of-flight analysis of the Ar beam. Two different nozzle assemblies as shown in Figures 2a and 2b have been compared: nozzle (a) is recessed 10 mm more into the heating coil than nozzle (b) to obtain a higher nozzle temperature. This effect can clearly be seen. Pushing the nozzle even further into the oven leads to a disturbance of the Ar expansion cloud and would reduce the beam intensity dramatically. It can

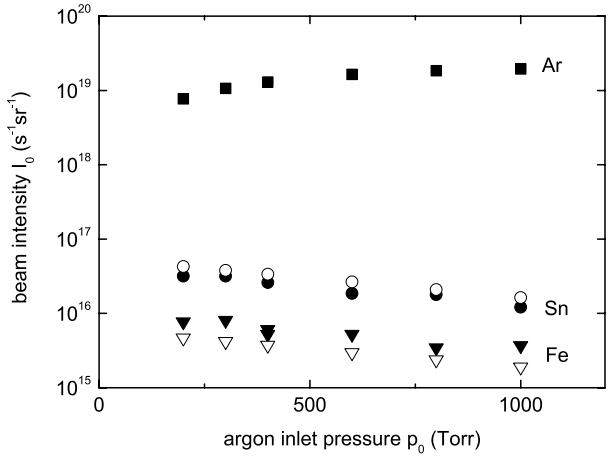

Fig. 6. Center line beam intensities I_0 of Ar, Fe and Sn at a nozzle temperature of 1930 K. Ar beam intensities are calculated using equation (7), the Fe and Sn beam intensities (closed symbols) are calculated by multiplying the Ar beam intensity with the ratio of the count rates of Fe or Sn to Ar. Open symbols represent more accurate values of the Fe and Sn beam intensities calculated by equation (11), using known values for the vapor pressure at 1930 K.

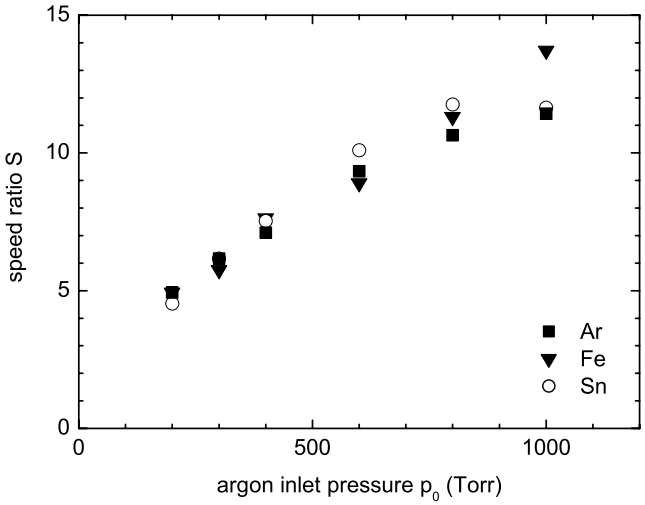

Fig. 7. Speed ratio S of Ar, Fe and Sn measured by TOF as a function of the inlet pressure p_0 at a nozzle temperature of 1930 K.

Table 2. Measured beam attenuation $\exp(-q'p_0)$ of the Ar, Fe and Sn beam due to collisions at the skimmer.

$q = 8.6 \times 10^{-4}$ torr^{-1}	q'/q (Eq. (11))	q'/q (Fig. 6)
Ar	1	1
Fe	1.35	1.33 ± 0.15
Sn	1.38	1.39 ± 0.1

also be seen that nozzle (a) is hotter than the reservoir temperature as a result of the thinner last winding of the graphite heating coil. Nozzle clogging does therefore not occur.

To demonstrate the performance of the source for different metals, Fe and Sn have been put into the Al_2O_3 crucible simultaneously. The center line beam intensities of Ar, Fe and Sn at an oven temperature of 1930 K are shown in Figure 6. It can be seen that the Ar beam intensity increases with increasing Ar inlet pressure p_0, but starts to saturate due to the exponential decay factor caused by beam attenuation at the skimmer. This causes the beam intensities of Fe and Sn to decrease exponentially. However, still more than 50% of the undisturbed intensity is left at 1000 torr inlet pressure. Calculating the exponential decay rates of Fe and Sn gives slightly different rates, as predicted by equation (11). Table 2 shows the results of the exponential beam attenuation of Ar, Fe and Sn, as measured in Figure 6.

The absolute values of the beam intensities of Fe and Sn are calculated in two ways: first by multiplying calibrated Ar intensities with the ratio of the detector beam signals of Fe and Sn to Ar. This approach naively assumes that the sensitivity of the detector is the same for all three species. A second and better estimate is to use equation (10). However, both estimates seem to result in a very good agreement for Sn and in a reasonable agreement (within a factor of 2) for Fe. Evidently, Fe beam intensities exceeding 10^{15} s^{-1} sr^{-1} can very well be achieved.

Increasing the oven temperature by 200 K results in a 10 fold increase of the beam intensities of Fe and Sn. However, a more intensive maintenance of the skimmer after approximately every 8 hours of operation is then necessary due to a very high deposition rate of Sn onto the skimmer tip. With only Fe in the crucible, the latter problem should not exist and Fe fluxes well exceeding 10^{16} could be achieved for long periods without maintenance.

The speed ratios of the Ar, Fe and Sn atoms have also been measured. Figure 7 shows the result of a measurement of a supersonic expansion at a nozzle temperature of 1930 K. The oven temperature has been determined together with the speed ratios by fitting the time of flight spectra with equation (12). It can be seen that the speed ratios increase with increasing Ar pressure to values well above 10 for Ar, Fe and Sn. The difference between Ar, Fe and Sn speed ratios is hardly discernable. From equation (9) it is to be expected that the Fe speed ratios should be the same as the Ar speed ratios, but the Sn speed ratios should be approximately 25% higher. However, the last aspect is not confirmed experimentally . The accuracy of these measurements is determined by the signal to noise ratio of the TOF data. This ratio is highest for argon, and lowest for Fe, in which case a signal to noise ratio of around 3 has been measured. As a result, the uncertainty in the speed ratio is approximately 10%. The speed ratio of Ar and Sn have been determined within 5% and 7% accuracy.

A more detailed series of measurement of speed ratios of Ar is shown in Figure 8. In these measurements the speed ratio of Ar has been determined at various nozzle temperatures in the range of 1200 to 2200 K. A good agreement with published values [16] represented by equations (5, 6) can be observed.

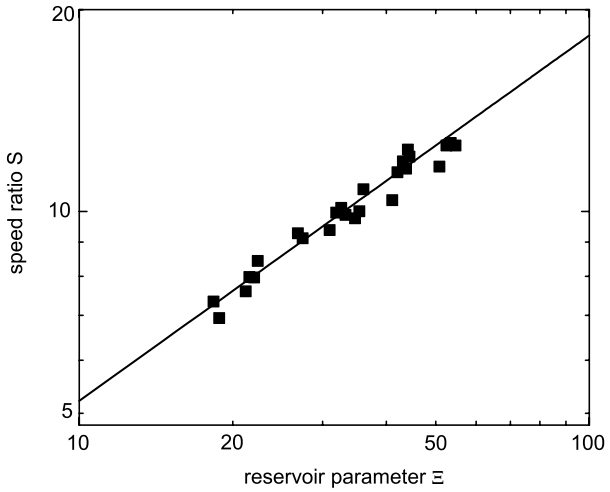

Fig. 8. Log-log plot of Ar speed ratios measured by TOF as a function of the reservoir parameter Ξ. The solid line represents published values represented by equation (5).

6 Conclusions

The presented high temperature evaporation source shows excellent performance for the generation of a supersonic Fe beam. Care has to be taken in the choice of the crucible materials to prevent difficulties with the reactive Fe atoms. The alumina crucible seems to suffer least from this restriction. The design allows the metal to be reloaded many times without damaging the crucible.

The properties of the Fe beam at a nozzle temperature of 1930 K have been determined. Beam intensities up to 5×10^{15} s^{-1} sr^{-1} can be achieved. Increasing the temperature by 200 K will increase the beam intensity by a factor of 10.

Increasing the argon inlet pressure to 1000 torr leads to a skimmer transmission still above 50%, thus not reducing the Fe beam intensity dramatically. At these higher pressures the beam monochromaticity is excellent, resulting in speed ratios well above 10. Speed ratios for argon are in agreement with earlier published values. Speed ratios for Fe are the same, as predicted theoretically.

Since a well defined Fe beam with controllable beam properties can be achieved, the presented supersonic Fe source shows great promise for future fabrication of nanomagnetic Fe structures.

The authors wish to thank O.F. Hagena for sharing his expertise on high temperature evaporation sources and for providing construction drawings that proved to be very useful for the development of our supersonic Fe beam source. This work is financially supported by the Dutch Foundation for Fundamental Research (FOM).

References

1. S.J.H. Petra, L. Feenstra, W. Vassen, W. Hogervorst, *Int. Quantum Electron. Conference CLEO/Europe-IQEC 2000, Nice, France*
2. B. Brezger, Th. Schulze, U. Drodofsky, J. Stuhler, S. Nowak, T. Pfau, J. Mlynek, J. Vac. Sci. Technol. B **15**, 2905 (1997)
3. P. Engels, S. Salewski, H. Levsen, K. Sengstock, W. Ertmer, Appl. Phys. B **69**, 407 (1999)
4. K.K. Berggren, A. Bard, J.L. Wilbur, J.D. Gillaspy, A.G. Helg, J.J. McClelland, S.L. Rolston, W.D. Phillips, M. Prentiss, G.M. Whitesides, Science **269**, 1255 (1995)
5. F. Lison, H.J. Adams, P. Schuh, D. Haubrich, D. Meschede, Appl. Phys. B **65**, 419 (1997)
6. G. Timp, R.E. Behringer, D.M. Tennant, J.E. Cunningham, Phys. Rev. Lett. **69**, 1636 (1992)
7. J.J. McClelland, R.E. Scholten, E.C. Palm, R.J. Celotta, Science **262**, 877 (1993)
8. R.W. McGowan, D. Giltner, Siu Au Lee, Opt. Lett. **20**, 2535 (1995)
9. F.J. Himpsel, J.E. Ortega, G.J. Mankey, R.F. Willis, Adv. Phys. **47**, 511 (1998)
10. M.D. Hoogerland, J.P.J. Driessen, E.J.D. Vredenbregt, H.J.L. Megens, M.P. Schuwer, H.C.W. Beijerinck, K.A.H. van Leeuwen, Appl. Phys. B **62**, 323 (1996)
11. H.C.W. Beijerinck, N.F. Verster, Physica C **111**, 327 (1981)
12. R.C.M. Bosch, Vacuum Solutions 17, March/April 2000
13. O.F. Hagena, Z. Phys. D **20**, 425 (1991)
14. J.B. Anderson, *Molecular beams and low density gas dynamics*, edited by P.P. Wegener (Dekker, New York, 1974), Vol. 1
15. R. Campargue, Rev. Sci. Instrum. **35**, 111 (1964)
16. H.C.W. Beijerinck, R.J.F. van Gerwen, E.R.T. Kerstel, J.F.M. Martens, E.J.M. van Vliembergen, M.R.Th. Smits, G.H. Kaashoek, Chem. Phys. **96**, 153 (1985)
17. D.R. Miller, R. Andres, Rarefied Gas Dynamics, *Proc. VI Symp.* (Academic Press, New York, 1969), Vol. 2, p. 1385
18. O.F. Hagena, G. Knop, R. Fromknecht, G. Linker, J. Vac. Sci. Technol. A **12**, 282 (1994)